Received: 14 June 2022 | Accepted: 14 February 2023

DOI: 10.1111/2041-210X.14082

Methods in Ecology and Evolution

RESEARCH ARTICLE

Reconstructing bird trajectories from pressure and wind data using a highly optimized hidden Markov model

Raphaël Nussbaumer[1,2] | Mathieu Gravey[3] | Martins Briedis[2,4] | Felix Liechti[2,5] | Daniel Sheldon[6]

[1]Cornell Lab of Ornithology, Ithaca, New York, USA; [2]Swiss Ornithological Institute, Sempach, Switzerland; [3]Department of Physical Geography, Faculty of Geosciences, Utrecht University, Utrecht, Netherlands; [4]Lab of Ornithology, Institute of Biology, University of Latvia, Riga, Latvia; [5]Swiss Birdradar Solutions AG, Winterthur, Switzerland and [6]University of Massachusetts Amherst, Amherst, Massachusetts, USA

Correspondence
Raphaël Nussbaumer
Email: ryn5@cornell.edu

Funding information
Schweizerischer Nationalfonds zur Förderung der Wissenschaftlichen Forschung, Grant/Award Number: 191138; Development of the Geolocators, Grant/Award Number: UTF-Nr. 254, 332, 363, 400

Handling Editor: Edward Codling

Abstract

1. Tracking technologies have widely expanded our understanding of bird migration routes, destinations and underlying strategies. However, determining the entire trajectory of small birds equipped with lightweight geolocators remains a challenge.
2. We develop a highly optimized hidden Markov model (HMM) for reconstructing bird trajectories. The observation model is defined by pressure and, optionally, light measurements, while the movement model incorporates wind data to constrain consecutive positions based on realistic airspeeds. To reduce the computational costs associated with a large state space, we prune the HMM states and transitions based on flight and observation constraints to efficiently model the entire trajectory.
3. The approach presented is based on a mathematically exact procedure and is fast to compute. We demonstrate how to compute (1) the most likely trajectory, (2) the marginal probability map of each stationary period, (3) simulated trajectories and (4) the wind conditions (wind support/drift) encountered by the bird during each migratory flight.
4. We construct a version of an HMM optimized for reconstructing a bird's migration trajectory based on lightweight geolocator data. To render this approach easily accessible to researchers, we designed a dedicated R package GeoPressureR (https://raphaelnussbaumer.com/GeoPressureR/).

KEYWORDS
animal tracking, animal-borne sensor, archival tags, biologger, bird migration, forward–backward, geolocation, graph, Hidden Markov Model, reanalysis data, wind drift, wind profit

1 | INTRODUCTION

Tracking technologies constitute an essential tool to better understand animal migratory movements and behaviour (Bridge et al., 2011; Kays et al., 2015). Indeed, by providing frequent information about an animal's position, they allow researchers to study the factors influencing the migratory route used (e.g. Briedis, Bauer, et al., 2020; Thorup et al., 2017). In addition, tracking a single individual during its full journey can reveal space–time interactions as well as cumulative effects over time (e.g. McKinnon et al., 2015).

Tagging small animals (<50 g) comes with strict requirements on the weight of the tracking device, limiting the type of technology used to lightweight devices. These devices are particularly suited to smaller bird species but can also be used more broadly on larger species in cases where satellite transmitters cannot be set. The two main technologies currently allowing to precisely position small birds include archival GPS (e.g. Hallworth & Marra, 2015) and automatic telemetry (e.g. Taylor et al., 2017). However, these only provide a limited number of position estimates. Beyond these two technologies, lightweight geolocators can provide regular positions with larger uncertainty by measuring environmental variables for which the spatiotemporal variation is known. Among these, light-level geolocators are the oldest and most widespread technology (Wilson et al., 1992), along with devices measuring sea-surface temperature used mostly for marine wildlife (e.g. Nielsen et al., 2006). More recently, location estimates based on atmospheric pressure sensors have been shown to provide positions with higher precision (Nussbaumer et al., 2023). This offers promising research avenues as pressure information becomes increasingly available with the use of multi-sensor geolocators (Bäckman, Andersson, Alerstam, et al., 2017; Bäckman, Andersson, Pedersen, et al., 2017; Dhanjal-Adams et al., 2018; Liechti et al., 2018; Sjöberg et al., 2018). Yet, both light- and pressure-based location estimates suffer from large uncertainty, particularly during the short stopovers that constitute critical steps in the migration trajectory.

Trajectory estimation from imperfect position data is a well-known problem in the animal movement literature and is typically modelled as a state-space model (SSM; e.g. Jonsen et al., 2013; Patterson et al., 2008), where the animal's position X_t is defined as a Markov model called a process or movement model $P(X_t | X_{t-1})$. The model considers that X is unknown but is related to an observed variable Y (e.g. light, pressure, or temperature measurements) through an observation model $P(Y_t | X_t)$. SSMs for light-level geolocators and sea-surface temperature have been mostly developed in marine biology and solved with a Kalman filter (Nielsen et al., 2006; Sibert et al., 2003) or an unscented Kalman filter (Lam et al., 2008; Nielsen & Sibert, 2007). However, when the SSM is strongly non-linear (e.g. with pressure geopositioning), a Kalman filter cannot be used and more computationally demanding Bayesian methods such as Markov Chain Monte Carlo (MCMC; Jonsen et al., 2005; Sumner et al., 2009) or particle filtering (Rakhimberdiev et al., 2015; Royer et al., 2005) must be employed. Such methods have been used successfully for reconstructing the trajectory of small birds using lightweight geolocation (e.g. Lisovski et al., 2020). However, their implementation can be challenging due to the complexity of choosing the type of Monte Carlo method, configuring the run (e.g. step size) and checking convergence. In this paper, we consider only the problem of estimating bird trajectories given the observations under a fixed process model. For the related problem of performing inference jointly over trajectories and unknown parameters of a process model, efficient routines for trajectory estimation can be nested within a larger inference procedure, for example, using MCMC.

Whenever the SSM can be discretized in space and time (e.g. Pedersen et al., 2011), it becomes a hidden Markov model (Rabiner, 1989). In such cases, the positions can be estimated exactly and efficiently with the forward–backward algorithm, also known as a two-pass recursive algorithm (Rabiner, 1989; Scott, 2002; Zucchini et al., 2017), and the mostly likely trajectory can be found with the Viterbi algorithm (Viterbi, 2006). These algorithms have been used in animal movement literature (Leos-Barajas & Michelot, 2018; McClintock et al., 2020; Patterson et al., 2016) but have rarely been applied to geolocator data (e.g. Bindoff et al., 2018). A major challenge in estimating the trajectory of a bird with this approach is the memory requirements to store the probabilities of every possible transition between pairs of locations using a data structure known as the trellis graph (e.g. Rabiner, 1989).

Using pressure data from the geolocator, the trajectory of the bird can be efficiently modelled as an hidden Markov model (HMM) because bird trajectories can be discretized in a limited number of periods (time) and grid cells (space). Unlike marine wildlife, most birds migrate by alternating active migratory flight with periods of residency (stationary periods), where their position can be assumed fixed at the precision level provided by light and pressure geopositioning (~10 km). In addition, identifying the exact duration of flights (using activity data or pressure) can inform the movement model of the SSM by constraining the distance between consecutive positions, assuming a distribution of ground speeds (e.g. Briedis, Beran, et al., 2020). In this context, wind data have recently been shown to considerably improve position estimates because of the strong influence of wind on a bird's ground speed (Werfeli et al., 2022).

In this study, we present a framework to reconstruct the trajectory of a bird based on pressure (and optionally light) data captured by geolocators. In this approach, we model the trajectory as a discrete SSM (or HMM) and optimize the trellis graph of the HMM, where nodes correspond to the position of the bird at a stationary period and edges represent transitions from one position to the next. We first explain how to efficiently build this trellis graph (Section 2.2) and then demonstrate how the graph can be used to (1) identify the trajectory that maximizes the overall probability with the Viterbi algorithm (Section 2.3.1), (2) compute a marginal probability map of the bird's location at each stationary period using the forward–backward algorithm (Section 2.3.2) and (3) simulate possible trajectories with the sequential simulation algorithm (Section 2.3.3). Finally, we show how wind support and drift can be computed for each flight of the trajectory (Section 2.4).

This method is available as an R package, called GeoPressureR (https://raphaelnussbaumer.com/GeoPressureR/), including a user manual, GeoPressureManual (https://raphaelnussbaumer.com/GeoPressureManual/) and an introductory code, GeoPressureTemplate (https://raphaelnussbaumer.com/GeoPressureTemplate/).

2 | MATERIALS AND METHODS

2.1 | Data

To illustrate how this method is implemented, we use a geolocator dataset consisting of 16 tracks from nine species covering a variety of migration distances and speeds. The dataset and its basic processing are described in full detail in Nussbaumer et al. (2023) and briefly recalled below.

First, the accelerometer and pressure data of each track are used to identify (1) stationary periods where the bird is assumed to be at a fixed location (~1–10 km scale) and (2) the time of departure and arrival for all flights. Then, using pressure data, we determine the likelihood map (i.e. the probability of observing the pressure measurements conditional to the position of the bird) on a discrete map of 0.25° (~27 km) resolution for each stationary period and each bird. Finally, we estimate the likelihood map from light data on the same map size and resolution as pressure. Knowing that pressure and light data are independent, the observation model is defined by the product of the pressure and light likelihood maps. If no light data are available, the methodology can be applied using the pressure likelihood map alone.

For the movement model, we rely on an external database of windspeed (ERA-5 pressure level dataset Hersbach et al., 2018a). Windspeed is used to refine the likelihood of the transition between each stationary period (see Section 2.2.5 for more details).

2.2 | Building the trellis graph

We model the trajectory of a single bird with an HMM by discretizing the positions $X_0, \ldots, X_n$ of the bird in $n+1$ stationary periods and relating these positions to the observations $Y_0, \ldots, Y_n$ of pressure (and optionally light) via the SSM

$$P(X_0, \ldots, X_n, Y_0, \ldots, Y_n) = P(X_0) \prod_{k=1}^{n} P(X_k | X_{k-1}) \prod_{k=0}^{n} P(Y_k | X_k). \quad (1)$$

The initial distribution $P(X_0)$ has little impact because the initial observation $P(Y_0 | X_0)$ strongly constrains inferences about X_0, for example, by encoding the known location of initial capture and tagging. As such, we assume $P(X_0)$ to have a uniform distribution over space. The transition probabilities $P(X_k | X_{k-1})$ will vary with time due to the different flight durations and the effect of wind. The possible positions in space are discretized according to the resolution of the likelihood map (0.25°). Note that we do not model additional state variables (e.g. behaviour). Building the full HMM of the trajectory would require computing and storing the transition probabilities between every pair of locations for each consecutive pair of stationary periods, a total of $(n_{lat}\, n_{lon})^2 n$ values. This is computationally feasible only for small grids as it would require both significant computational effort and large memory.

Many positions on the grid are unlikely according to the observation model, and most transitions are unlikely according to the movement model. Thus, some minor simplifications can dramatically reduce the number of transitions. In such cases, it becomes more convenient to represent the HMM via its trellis graph, where the nodes represent the possible position of the bird at each stationary period and the edges correspond to the transition of the bird from one node to the next (e.g. Rabiner, 1989). The probability of the observation model can be conveniently encoded at the node level, while the probability of the movement model can be associated with edges.

The computational feasibility of constructing such a graph still relies on careful considerations. To maximize computational efficiency and minimize memory requirements, we follow a five-step process to create the graph. The aim of the first two steps is to reduce the number of nodes and thereby avoid computing excessively numerous transitions. Once only likely nodes remain, we compute the edges and prune the graph with computationally demanding operations (e.g. windspeed; steps 3–5). The steps are explained in detail below and illustrated in Figure 1.

2.2.1 | Step 1: Constructing the nodes with the observation model

We keep all the nodes of the graph up to the 99th percentile of the likelihood maps of the observation model. These nodes correspond to the coloured pixels of the likelihood map of pressure and light data in Figure 1b. If the first and/or last stationary periods are known (equipment/retrieval site), they are assigned a probability of 1 at their known location and 0 everywhere else.

2.2.2 | Step 2: Pruning nodes with the movement model

We compute the maximum flight distance possible between each stationary period $D(k, k+1)$ using the flight duration estimated from pressure data (see Section 2.1) and a ground speed threshold of 150 km/h. This threshold allows for exceptionally high speeds as the 95th percentile of ground speed for small migratory birds is below 90 km/h (Liechti & Bruderer, 1995). Nodes that are too far from any other nodes from either the previous or the following stationary period are pruned.

For computational feasibility, it is critical to perform this pruning without doing a full pairwise comparison among all nodes. More specifically, let m_k ($m_k < n_{lat} n_{lon}$) be the number of active (i.e.

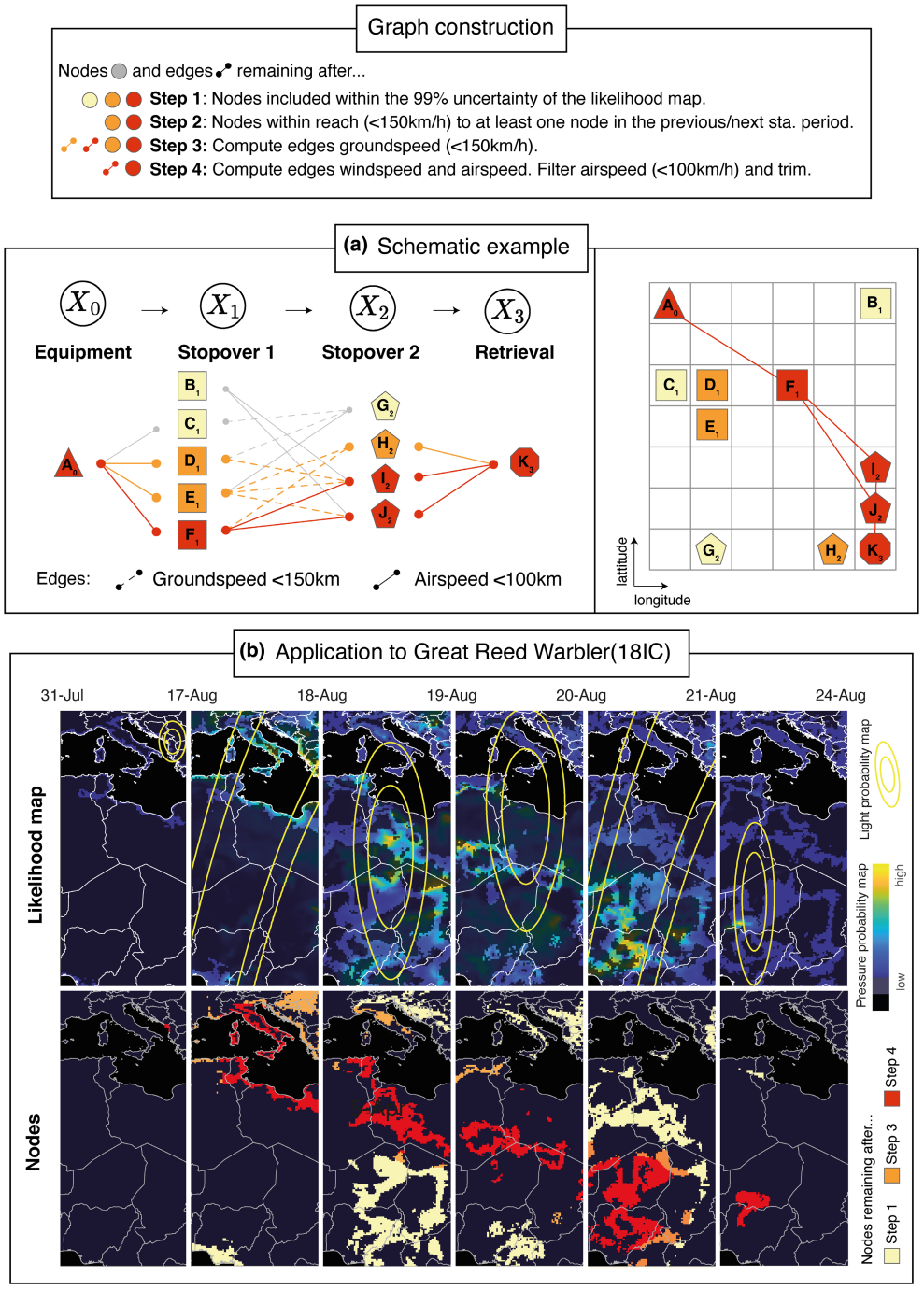

FIGURE 1 Illustration of the creation of the graph. (a) The schematic example considers a simple trajectory from an equipment site (A_0) to a retrieval site (K_3) in three flights and two stationary periods. Nodes of different stationary periods are overlayed on the same spatial grid (right panel) (but distinguishable by subscript and shape). **Step 1**. We keep all nodes corresponding to possible positions according to the 99th percentile of the likelihood map. We do not illustrate the static probability map for the schematic example. **Step 2**. We eliminate nodes that are not within reach (<150 km/h) of at least one node from the previous and following stationary period. B_1 is eliminated on the forward pass, G_2 and C_1 are eliminated on the backward pass. **Step 3**. We construct all possible transitions (red and orange lines). **Step 4**. After computing the average windspeed and airspeed for each transition, we prune edges requiring an airspeed >100 km/h (orange dotted line). The final graph is thus composed of the red nodes and edge. (b) An example of the application of the method using the same subset of stationary periods as in fig. 4 in Nussbaumer et al. (2023).

non-pruned) nodes for stationary period k after Step 1. A naïve algorithm to execute the pruning of this step would require the order of $m_k m_{k+1}$ computational steps, for example, by checking if each active node in stationary period k is within the maximum flight distance of at least one active node in stationary period $k + 1$. However, we perform the same operation in time proportional *only to* m_k (i.e. time

linear in the currently active number of nodes), which enables a significant speedup. We do this by using a fast algorithm for distance transformations in binary images (i.e. 0/1-valued; e.g. Kolountzakis & Kutulakos, 1992; Maurer et al., 2003). A distance transformation computes the distance between every pixel and the closest pixel with a '1' value, which, in our setting, represents currently active nodes in stationary period k. The algorithm uses the Euclidian distance on the image coordinates (i.e. lat-lon). These distances in decimal degrees are converted into kilometres assuming a flat-earth surface while accounting for the variation of distance between meridians ($d_{km} = 111 \times \cos(\text{lat}) \times d_{deg}$).

Using the distance transformation from the active nodes in stationary period k, we prune the active nodes for stationary period $k+1$ requiring a flight distance higher than the maximum flight distance $D(k, k+1)$. This operation is repeated for all pairs of stationary periods going forward and then backward to ensure that all nodes are connected to the first and last nodes (equipment and retrieval). This efficient pruning relies on the specific structure of the HMM, in which the states are located on a regular grid, allowing them to be treated as a binary image.

2.2.3 | Step 3: Computing edges with ground speed

Having identified and pruned the nodes, we now compute all edges between the remaining nodes. We compute the ground speed for each edge using the great circle distance and the duration of the flight.

Then, we filter the edges with the threshold of 150 km/h, which also removes some nodes as the flat-earth distance used in Step 2 was approximate. Finally, we prune the graph based on the constraint that all nodes must be connected to both the equipment and retrieval nodes using the breadth-first search algorithm (Cormen et al., 2022).

2.2.4 | Step 4: Computing edges with airspeed

We compute the average windspeed and airspeed of all edges and prune the graph based on a predefined airspeed threshold of 100 km/h, which considers potential uncertainty in wind estimates as the 95th percentile of airspeed for small bird migrants is below 75 km/h (Liechti & Bruderer, 1995).

To account for spatiotemporal change in windspeed at short temporal scales (especially with altitude), we take advantage of knowing, for each edge of the graph, (1) the exact time of departure and arrival (see Section 2.1), (2) the location of departure and arrival, and (3) the geolocator pressure measurements during the flight, which correspond to the bird's altitude.

We use the E/W and N/S windspeed components from the ERA5 pressure levels dataset (Hersbach et al., 2018a), which provide hourly wind estimates at a spatial resolution of 0.25° in latitude and longitude at 37 different pressure levels (i.e. altitudes). We then proceed to build two 4D gridded linear interpolations (E/W and N/S) that provide an estimate of windspeed for any time, latitude, longitude and pressure level.

For each edge of the graph, we estimate the average windspeed encountered by the bird. We construct the flight trajectory of the bird with discrete 4D positions (time–latitude–longitude–pressure level) as follows:

- We discretise the trajectory on an hourly basis starting on the hour preceding flight departure and ending on the hour following arrival.
- The latitude and longitude positions are estimated assuming a linear displacement (i.e. "as the crow flies") between the departure and the arrival nodes.
- The pressure level positions are retrieved from the geolocator pressure measurements.

Windspeed significantly contributes to the displacement of the bird and can vary considerably within a flight. We, therefore, correct the horizontal position of the bird to assume a constant airspeed rather than a constant ground speed which would correspond to equally spaced hourly positions. We use an approximate two-step approach.

In the first step, we initialize the position assuming a constant ground speed G and query the corresponding hourly windspeed w_i. We can then compute the average airspeed of the flight with $A = G - \frac{1}{n}\sum_i^n w_i$. Then, the hourly ground speed can be estimated with $g_i = A + w_i$. Finally, we adjust the hourly position based on the hourly ground speed. In the second step, the hourly windspeeds w_i are now queried at the adjusted positions and used to compute the average windspeed of the flight $W = \frac{1}{n}\sum_i^n w_i$. We can compute the average airspeed of the total flight as $A = G - W$. All these operations are performed with vectorial speed (lat-lon) and the trapezoidal rule is used in the weighting of the average to account for the exact time of departure and arrival.

Finally, we prune the graph similarly to the previous step, this time based on an airspeed threshold of 100 km/h.

2.2.5 | Step 5: Computing the transition probabilities

In the final step, we compute the transition probability $P(X_t \mid X_{t-1})$ (i.e. movement model) for each edge from the airspeed. We define a parametric function converting the average airspeed into a probability using flight energetics and considering that a bird is more likely to fly at an airspeed resulting in lower energy consumption. More specifically, we empirically define the probability proportional to the cubic inverse of the mechanical power of flight P_{mech} of the airspeed v_a,

$$P(X_k = x_k \mid X_{k-1} = x_{k-1}) \propto \left(\frac{1}{P_{mech}\left(\max\left(v_a\left(x_{k-1} \to x_k\right), v_{lim}\right)\right)} \right)^3, \quad (2)$$

where $v_a(x_{k-1} \to x_k)$ is the airspeed computed in step 4 for the edge of the transition from the node x_{k-1} to the node x_k. The mechanical power is computed with FlightMAT (Nussbaumer, 2022) following Pennycuick (2008), and taking into account each species' mass, wingspan and wing area from Tobias et al. (2022). We additionally impose a minimum apparent airspeed of v_{lim}=5 km/h, which allows for birds to perform short exploratory flights (e.g. Mills et al., 2011; Schmaljohann et al., 2011).

2.3 | Trajectory outcomes

Using the constructed graph, we derive the following three outcomes.

2.3.1 | Most likely trajectory

While the mean or median positions of each stationary period are commonly used to illustrate a single trajectory, they do not adequately represent the connectivity between stationary periods, even more so when the probability map is multi-modal. Instead, we suggest using the most likely trajectory, corresponding to the trajectory maximizing the joint probability,

$$\arg\max_{x_0,\dots,x_n} P(X_0 = x_0, \dots, X_n = x_n, Y_0 = y_0, \dots, Y_n = y_n).$$

Within graph theory, the shortest path problem is a well-known computational task seeking to identify the path characterized by the smallest sum of weights of all its edges. The most likely trajectory is equivalent to the shortest path when the weights of the edges are defined as the negative log of the probability. Using this formulation, we compute the most likely trajectory using the shortest path search with Dijkstra's algorithm (Dijkstra, 1959). This operation produces the same result as the Viterbi algorithm for finding the single best state sequence in an HMM (Rabiner, 1989; Viterbi, 2006).

2.3.2 | Marginal probability maps

We take advantage of the compact sparse graph to compute the marginal probability map of each stationary period, which is represented by the distribution $P(X_t | Y_0, \dots, Y_n)$ for each time step t. We use the forward–backward algorithm (e.g. Rabiner, 1989; Zucchini et al., 2017), which is a special case of the sum-product algorithm (e.g. Ross, 2019) tailored to HMMs.

We briefly explain how the forward–backward algorithm is applied in our case. For convenience, we group the transition probabilities $P(X_t | X_{t-1})$ into a transition matrix $\boldsymbol{T}_t$ $(m \times m)$, and all observation likelihoods $P(Y_t = y_t | X_t = x_t)$ for all values of $x_t$and for the observed value of y_t into the diagonal matrix $\boldsymbol{O}_t$ $(m \times m)$. Using the Chapman–Kolmogorov equation, we define the forward probability vector $\mathbf{f}_k$ and backward probability vector $\mathbf{b}_k$$(m \times 1)$ recursively,

$$\begin{aligned} \mathbf{f}_k^\mathsf{T} &= \mathbf{f}_{k-1}^\mathsf{T}(\boldsymbol{T}_k \boldsymbol{O}_k) \\ \mathbf{b}_{k-1} &= (\boldsymbol{T}_k \boldsymbol{O}_k)\mathbf{b}_k \end{aligned} \quad (3)$$

Starting with the forward probability vector $\mathbf{f}_0^\mathsf{T} = \boldsymbol{P}_0^\mathsf{T}\boldsymbol{O}_o$, which has entries of the form $P(X_0 = x_0)P(Y_0 = y_0 | X_0 = x_0)$ for each starting location x_0, and the vector $\mathbf{b}_n = \mathbf{1}$, (all ones, $m \times 1$), we can write the forward and backward probability vectors as

$$\begin{aligned} \mathbf{f}_t^\mathsf{T} &= \mathbf{f}_0^\mathsf{T}\boldsymbol{T}_1\boldsymbol{O}_1 \dots \boldsymbol{T}_t\boldsymbol{O}_t \\ \mathbf{b}_t &= \boldsymbol{T}_{t+1}\boldsymbol{O}_{t+1} \dots \boldsymbol{T}_n\boldsymbol{O}_n\boldsymbol{b}_n \end{aligned}, \quad (4)$$

The final vector $\boldsymbol{\mu}_t$ $(m \times 1)$ has entries of the form $P(X_t = x_t | Y_0, \dots, Y_n)$ corresponding to the marginal probabilities for each location. It is computed as the probability vector proportional to the element-wise product (denoted ∘) of the forward and backward probability vectors:

$$\boldsymbol{\mu}_t \propto \mathbf{f}_t \circ \mathbf{b}_t. \quad (5)$$

Following the same reasoning as the forward–backward algorithm, the marginal probability matrix $\boldsymbol{M}_{t-1,t}$ $(m \times m)$ of each transition (also called a pairwise marginal), which has entries $P(X_{t-1} = x_{t-1}, X_t = x_t | Y_0, \dots, Y_n)$, can be computed as

$$\boldsymbol{M}_{t-1,t} \propto \mathrm{diag}(\mathbf{f}_{t-1})\boldsymbol{T}_t\boldsymbol{O}_t\mathrm{diag}(\mathbf{b}_t). \quad (6)$$

2.3.3 | Random trajectories generator

To compute quantities relying on the entire trajectory such as the total distance flown or the average airspeed, it is most convenient to generate multiple possible trajectories and compute aggregated quantities on each one.

We use the forward filtering backward sampling (e.g. Carter & Kohn, 1994) to generate a possible trajectory $\boldsymbol{x} = (\boldsymbol{x}_0, \dots, \boldsymbol{x}_n)$ using the following steps:

1. Fix the known position of retrieval $\boldsymbol{x}_n$, or if unknown, sample from $\boldsymbol{\mu}_n$.
2. For each stationary period $k < n$, in a backward order,

1. Sample a position $\boldsymbol{x}_k$ given $\boldsymbol{x}_{k+1}$ from the probability vector proportional to $\mathbf{f}_k \circ \mathbf{1}_{\boldsymbol{x}_{k+1}}\boldsymbol{T}_k$, where the operator $\mathbf{1}_{\boldsymbol{x}_{k+1}}$ is used to extract the row of $\boldsymbol{T}_k$ corresponding to $\boldsymbol{x}_{k+1}$. The forward vector $\mathbf{f}_k$ is assumed to be already computed from Section 2.3.2.

2.4 | Wind analysis

The resulting position estimates are precise and accurate enough in relation to the spatial variation of wind to allow for studying wind conditions during flight. As ground speed, windspeed and airspeed have already been computed for each edge of the graph, we can easily extract and summarize their distributions from the randomly simulated

trajectories (Section 2.3.3). In addition to ground speed, airspeed and windspeed, we compute the distribution of wind support and drift by calculating the windspeed projection along each individual flight's orientation (wind support) and perpendicular to it (drift).

We qualitatively assess the relationship between each flight in terms of distance and orientation, as well as the direction and magnitude of wind. In addition, we characterize the overall effect of wind on the full trajectory by integrating the ground speed, windspeed, airspeed, wind support and drift over all flight durations to quantify the total displacement caused by each one.

3 | RESULTS

3.1 | Trajectory outcomes

The most likely trajectory, the marginal probability maps, and the simulated trajectories are illustrated in Figure 2 for six individuals of different species. Figures for all 16 tracks are available in Supporting Information 1 and https://doi.org/10.6084/m9.figshare.21731888. The probability map of each stationary period shows an irregular shape (i.e. not ellipsoidal) due to the pressure threshold and land mask (e.g. stopover in Italy for 18IC). The uncertainty is generally significantly smaller for long stationary periods (e.g. stopover in northern Tunisia for 18IC). The most likely trajectory connects each stationary period by finding the optimal compromise between generally minimizing the flight distance while preserving the stopover location in the most likely area. The most likely trajectory is expected to produce a realistic full trajectory, which is not guaranteed by alternatives such as using the average or median position of the marginal probability at each stationary period. The simulations, on the other hand, are useful to illustrate all the possible trajectories that the bird might have taken and thus visually represent the uncertainty in the overall trajectory.

3.2 | Wind analysis

Using the high-resolution trajectories produced, we can quantify the speed and direction of wind experienced during each flight.

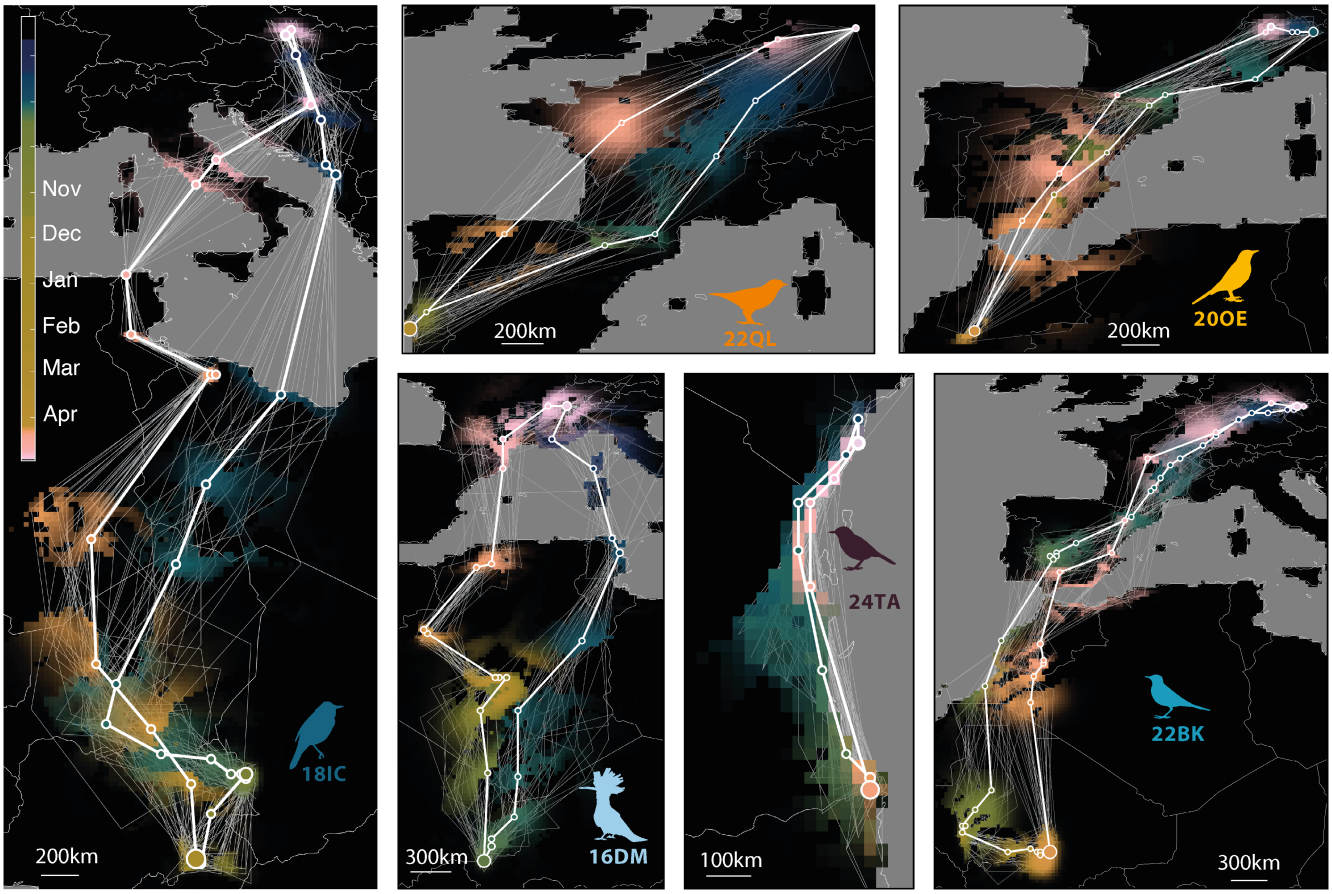

FIGURE 2 Illustration of the three outputs of this method for six birds (Great Reed Warbler 18IC; Eurasian Wryneck 22QL; Ring Ouzel 20OE; Eurasian Hoopoe 16DM; Red-capped Robin-chat 24TA; Tawny Pipit 22BK). (1) The coloured areas indicate the marginal probability of positions for each stationary period, with the colour indicating the time of year and the colour intensity indicating the value of the probability. Note that for visual purposes, we normalized the probability map of each stationary period separately. (2) The thick white line with circles represents the most-likely trajectory. (3) The thin white lines represent 30 simulations of possible trajectories. Higher-resolution maps for all 16 tracks are available in Supporting Information 1.

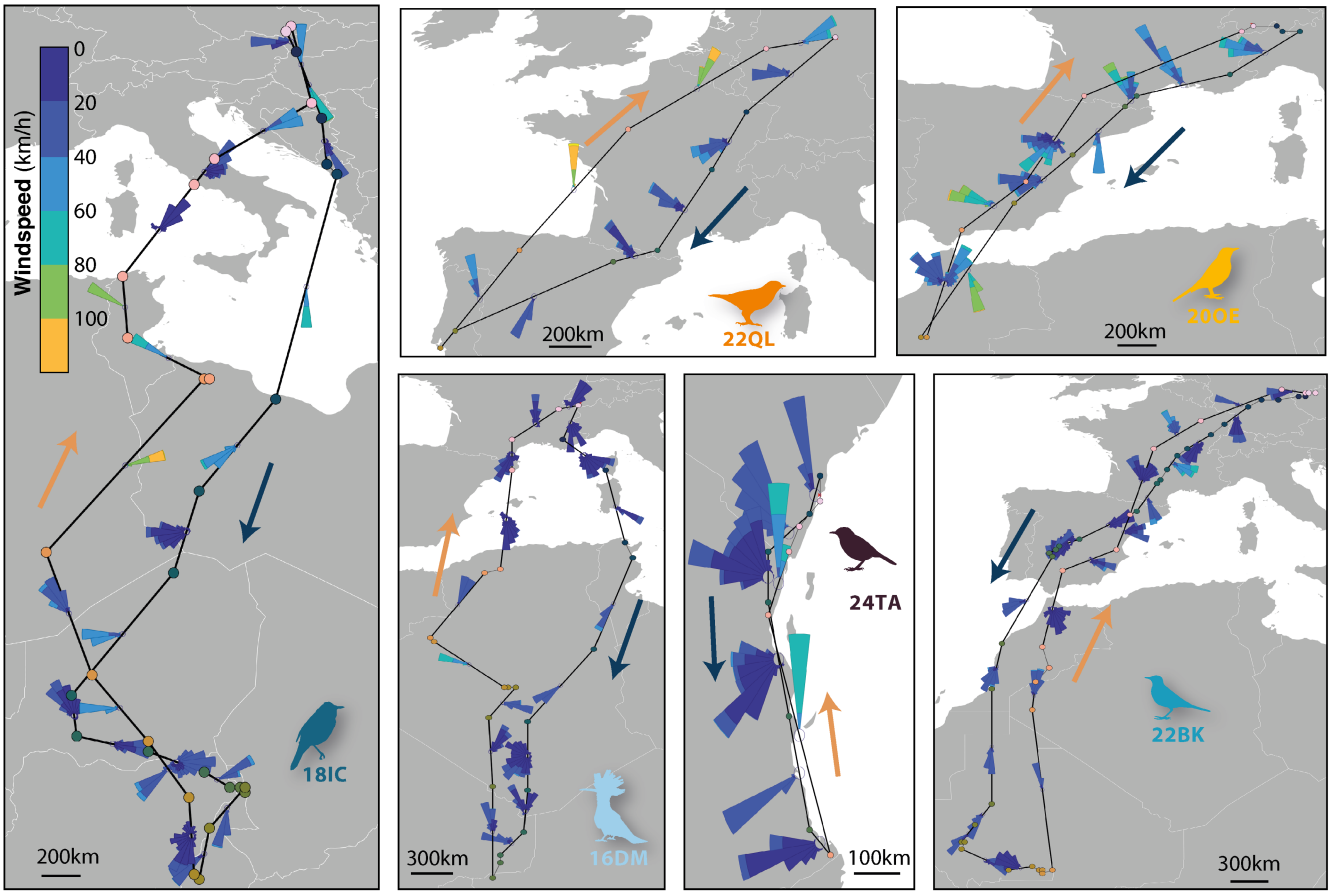

FIGURE 3 Wind rose plot of the windspeed distribution for each flight of more than 3 h computed from the 1000 simulations. The trajectory line illustrated represents the most likely trajectory. Note that the bin height (diameter of each wind rose) is normalized for each flight stage. Arrows indicate post- (blue) and pre-(orange) breeding migration. Higher-resolution maps for all 16 tracks are available in Supporting Information 2.

We illustrate the potential of this new approach by overlying the wind rose onto the most likely trajectory (Figure 3 and Supporting Information 2). Histograms of ground speed, windspeed and airspeed for each flight stage are available in Supporting Information 4. All flights generally occurred with supporting wind, and stronger wind support tends to be associated with longer flights and longer distance travelled. Northward migration (i.e. temperate spring except for intra-African migrants) is performed in fewer and longer flights as birds experience stronger wind support than during southward migration.

Interestingly, most detours in the trajectory can be explained by birds drifting while following the direction of strong supporting winds, such as the detour via Libya by 18IC, or the detour via western Algeria by 16DM, both during pre-breeding migration.

As illustrated above, wind can help birds reach their destination faster, but also cause lateral drift. We quantified the displacement due to the wind (windspeed) and due to the bird's own power (airspeed) for each flight of each track (Figure 4a and Supporting Information 3). To illustrate the benefit of incorporating windspeed data in the movement model, we highlight the longest non-stop flight of the Great Reed Warbler (18LX), lasting 20 h and covering about 2700 km. This impressive groundspeed (135 km/h on average) is largely explained by the high windspeed of 81 km/h, resulting in a reasonable airspeed of 54 km/h (Figure 4a).

Summing the displacement due to wind and airspeed for all flights in spring and autumn separately, we can compare the influence of wind between season and species. Except for the Eurasian Nightjar, long-distance migrants tend to be more efficient at maximizing wind support while minimizing drift compared to short-distance migrants (Figure 4b). In autumn, drift tends to be larger, and wind support smaller, than in spring while the overall distance travelled is greater.

4 | DISCUSSION

4.1 | Model strengths

In this paper, we present an approach to estimate the full migratory trajectory of a bird equipped with a lightweight geolocator. We model the trajectory as an HMM using a trellis graph, which, thanks to its compact format, allows us to efficiently build and store the full probability distribution of the trajectory. The model allows us to make inferences about the trajectory – such as computing the most likely trajectory or marginal probability maps – in

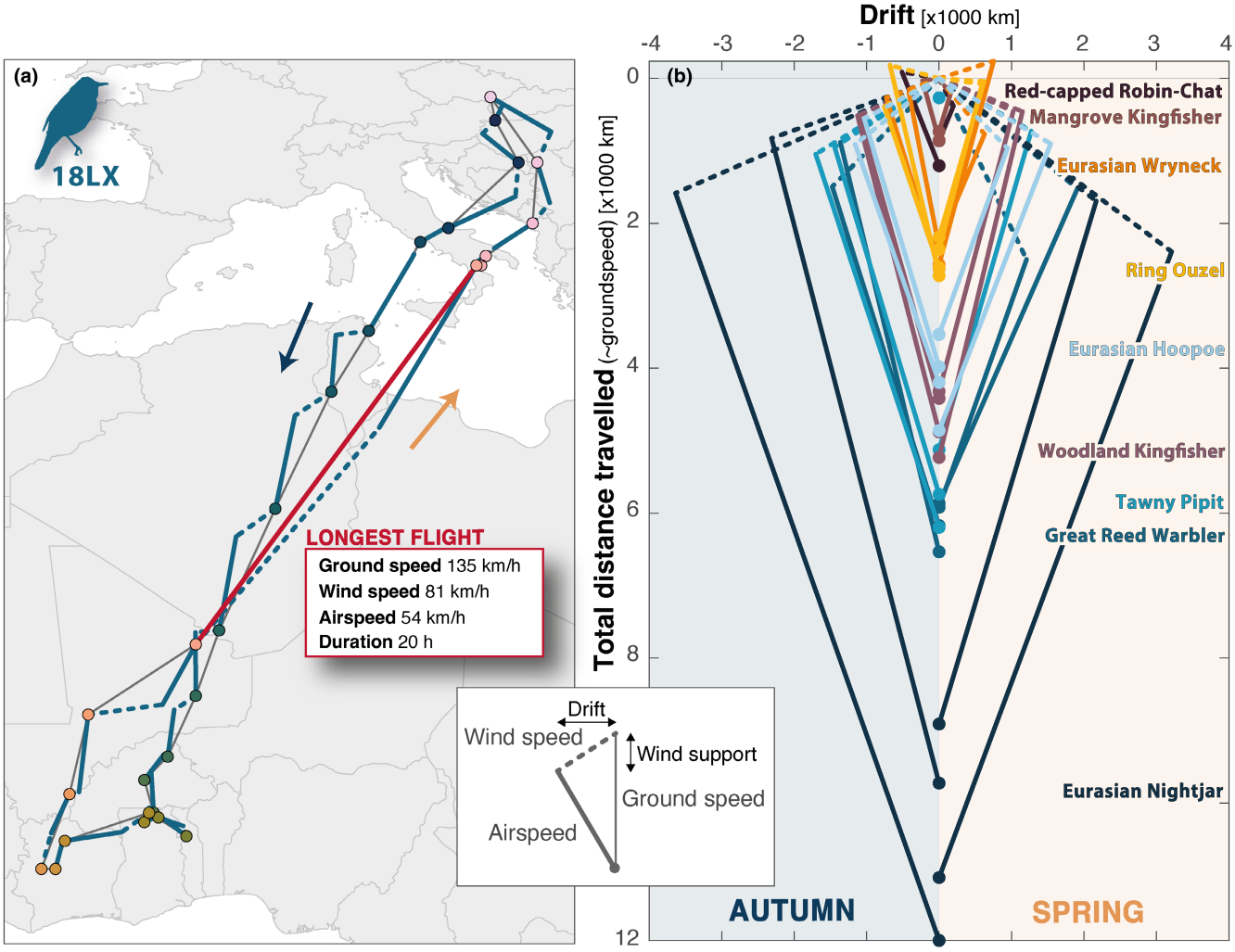

FIGURE 4 (a) Distance travelled by the Great Reed Warbler (18LX) propelled by wind (dotted line) and its own airspeed (continuous line) for each flight. The longest flight is highlighted in red to illustrate that the impressive ground speed (135 km/h) is mostly explained by the high windspeed (81 km/h). Similar maps for all 16 tracks are available in Supporting Information 3. (b) Illustration of the wind triangle of distance (rather than the usual wind triangle of speed) for spring (left) and autumn (right) migration. The total distance travelled (i.e. sum of all individual flights) (dot ~ ground speed) is the vectorial sum of the wind (dotted line ~ windspeed) and bird power (continuous line ~ airspeed). This representation allows to visually appraise the relative influence of the bird's drift (*x*-axis) and wind support (projection of the dotted line on the *y*-axis).

a mathematically exact manner (up to pruning of very low probabilities) while keeping computational costs low (see running time in Supporting Information 5).

Thanks to the high precision it provides, this framework can incorporate all stationary periods that make up the migration trajectory, even those lasting less than 12 h. The trajectory offers an elegant way to constrain the position of short stationary periods by combining the informative likelihood map (pressure and/or light) of long stationary periods with a realistic flight model. Information on the location and timing of such short stopovers can refine our understanding of migratory strategies and inform conservation measures by identifying the resting sites required by birds, even those visited for a short period.

In addition, the graph structure allows us to efficiently account for wind data to refine the possible distance covered by a bird, and ultimately improve the accuracy and precision of the trajectory. Compared to Werfeli et al. (2022), the computation of wind is further improved by integrating the variation of windspeed over time, space, and altitude encountered throughout the flight.

4.2 | Data requirements

This approach was developed and optimized for data collected from lightweight pressure sensors equipped on small birds. However, it could be applied to other datasets, under certain conditions. The observation model can incorporate any data that provide a position estimate. For instance, it can be based on light data only, possibly requiring a lower grid resolution. The approach can also integrate external information, such as field observations of the equipped

bird or data from archival GPS or telemetry. The method does not require knowledge of the position at the first or last stationary period (e.g. 22BK); however, this information can drastically reduce the size of the trellis graph. Additionally, the data collected by the device must provide the information needed to identify stationary periods and estimate flight duration. In the case of bird migration, this can be achieved using pressure measurements alone thanks to their high-altitude flight (e.g. Rhyne & Nussbaumer, 2022; Rime & Nussbaumer, 2022). Accelerometer data can be particularly helpful for this task because of its high temporal resolution. Wind data provide a facultative but significant improvement in the accuracy of possible flight distance. In the absence of wind data, the movement model (Section 2.2.5) should be replaced by a parametric equation of the ground speed (e.g. Briedis, Beran, et al., 2020).

Beyond birds, this approach could in theory be used to model the trajectory of other animals, provided they alternate between short periods of movement and extended periods of stationarity, where the animal can be assumed to remain in the same position relative to the grid resolution. Indeed, the modelling approach relies on the location of the bird being discretized in space and time over a finite number of stationary periods. This is typically not the case among most marine wildlife nor mammals.

For this approach to be applied successfully in other studies, the importance of high-quality labeling of pressure cannot be overstated (Nussbaumer et al., 2023), as a small labeling error could result in erroneous trajectory estimation. To avoid this, we recommend using the R Shiny app GeoPressureViz (https://raphaelnussbaumer.com/GeoPressureManual/geopressureviz.html), which helps researchers to visualize the full trajectory of the bird and validate the labeling and overall coherence of the likelihood maps with the movement model.

4.3 | Wind analysis

With precise position estimates for each stationary period and the high-resolution windspeed database, we can estimate the speed and direction of wind experienced by a bird with relatively high confidence. Consequently, wind support, airspeed and wind compensation can all be quantified on an individual level for small-bodied passerines. Our preliminary results from these 16 tracks qualitatively illustrate the significance of wind strength and direction in explaining flight distance, duration, and even the migration trajectory. As the objective of this paper is to describe the method used to reconstruct the trajectory, we do not investigate further ecological research questions here.

4.4 | GeoPressureR

Recent years have seen a growing number of studies using multi-sensor geolocators to track small-bodied passerine migrants (e.g. Liechti et al., 2018; Meier et al., 2018; Sjöberg et al., 2021). To assist researchers in applying this method to their own study, we developed the R package GeoPressureR (https://raphaelnussbaumer.com/GeoPressureR/) to (1) compute positions based on pressure (Nussbaumer et al., 2023), (2) build the graph and (3) compute the four outputs of this study. The package is accompanied by the user guide GeoPressureManual (https://raphaelnussbaumer.com/GeoPressureManual/) providing step-by-step explanations using the example of the Great Reed Warbler (18LX). Furthermore, the GitHub template repository GeoPressureTemplate (https://github.com/Rafnuss/GeoPressureTemplate) helps researchers kick-start their study with a pre-built folder structure, R code, and an automatically generated website report. Together, these tools aim to make the method described above accessible to all researchers and applied to a wide range of species, including birds and bats.

AUTHOR CONTRIBUTIONS

Raphaël Nussbaumer and Mathieu Gravey conceived the ideas and designed the methodology; Felix Liechti collected the data; Raphaël Nussbaumer performed the numerical implementation and analysis; Raphaël Nussbaumer created the figures and wrote the original draft; Felix Liechti, Daniel Sheldon and Martins Briedis reviewed and edited the manuscript. All authors contributed critically to the drafts and gave final approval for publication.

ACKNOWLEDGEMENTS

This research was funded by the Swiss National Science Foundation (grant no. 191138). The Swiss federal office for environment contributed financial support for the Development of the Geolocators (UTF-Nr. 254, 332, 363, 400). We are grateful to our colleagues from the Swiss Ornithological Institute Steffen Hahn, Silke Bauer, Michael Schaub and to our external collaborators Arnaud Barras, Ruben Evans, Samuel Temidayo Osinubi, Petr Prochazka and Dirk Tolkmitt for sharing their data with us. Data from Hersbach et al. (2018a, 2018b) were downloaded from the Copernicus Climate Change Service (C3S) Climate Data Store (https://cds.climate.copernicus.eu). The results contain modified Copernicus Climate Change Service information 2020. Neither the European Commission nor ECMWF is responsible for any use that may be made of the Copernicus information or data it contains.

CONFLICT OF INTEREST STATEMENT

The authors have no conflicts of interest to declare.

PEER REVIEW

The peer review history for this article is available at https://www.webofscience.com/api/gateway/wos/peer-review/10.1111/2041-210X.14082.

DATA AVAILABILITY STATEMENT

The code and datasets supporting the conclusions of this article are available at https://doi.org/10.5281/zenodo.7591132. This study used the MATLAB code GeoPressureMAT (https://github.com/Rafnuss/GeoPressureMAT). The same analysis can now be

performed with the R package GeoPressureR (https://raphaelnussbaumer.com/GeoPressureR/).

ORCID

Raphaël Nussbaumer https://orcid.org/0000-0002-8185-1020
Mathieu Gravey https://orcid.org/0000-0002-0871-1507
Martins Briedis https://orcid.org/0000-0002-9434-9056
Felix Liechti https://orcid.org/0000-0001-9473-0837
Daniel Sheldon https://orcid.org/0000-0002-4257-2432

REFERENCES

Bäckman, J., Andersson, A., Alerstam, T., Pedersen, L., Sjöberg, S., Thorup, K., & Tøttrup, A. P. (2017). Activity and migratory flights of individual free-flying songbirds throughout the annual cycle: Method and first case study. *Journal of Avian Biology*, *48*(2), 309–319. https://doi.org/10.1111/jav.01068

Bäckman, J., Andersson, A., Pedersen, L., Sjöberg, S., Tøttrup, A. P., & Alerstam, T. (2017). Actogram analysis of free-flying migratory birds: New perspectives based on acceleration logging. *Journal of Comparative Physiology A: Neuroethology, Sensory, Neural, and Behavioral Physiology*, *203*(6–7), 543–564. https://doi.org/10.1007/s00359-017-1165-9

Bindoff, A. D., Wotherspoon, S. J., Guinet, C., & Hindell, M. A. (2018). Twilight-free geolocation from noisy light data. *Methods in Ecology and Evolution*, *9*(5), 1190–1198. https://doi.org/10.1111/2041-210X.12953

Bridge, E. S., Thorup, K., Bowlin, M. S., Chilson, P. B., Diehl, R. H., Fléron, R. W., Hartl, P., Kays, R., Kelly, J. F., Robinson, W. D., & Wikelski, M. (2011). Technology on the move: Recent and forthcoming innovations for tracking migratory birds. *Bioscience*, *61*(9), 689–698. https://doi.org/10.1525/bio.2011.61.9.7

Briedis, M., Bauer, S., Adamík, P., Alves, J. A., Costa, J. S., Emmenegger, T., Gustafsson, L., Koleček, J., Krist, M., Liechti, F., Lisovski, S., Meier, C. M., Procházka, P., & Hahn, S. (2020). Broad-scale patterns of the Afro-Palaearctic landbird migration. *Global Ecology and Biogeography*, *29*(December 2019), geb.13063. https://doi.org/10.1111/geb.13063

Briedis, M., Beran, V., Adamík, P., & Hahn, S. (2020). Integrating light-level geolocation with activity tracking reveals unexpected nocturnal migration patterns of the tawny pipit. *Journal of Avian Biology*, *51*(9), 1–10. https://doi.org/10.1111/jav.02546

Carter, C. K., & Kohn, R. (1994). On Gibbs sampling for state space models. *Biometrika*, *81*(3), 541–553. https://doi.org/10.1093/biomet/81.3.541

Cormen, T. H., Leiserson, C. E., Rivest, R. L., & Stein, C. (2022). *Introduction to algorithms*. MIT press.

Dhanjal-Adams, K. L., Bauer, S., Emmenegger, T., Hahn, S., Lisovski, S., & Liechti, F. (2018). Spatiotemporal group dynamics in a long-distance migratory bird. *Current Biology*, *28*(17), 2824–2830.e3. https://doi.org/10.1016/j.cub.2018.06.054

Dijkstra, E. W. (1959). A note on two problems in connexion with graphs. *Numerische Mathematik*, *1*(1), 269–271. https://doi.org/10.1007/BF01386390

Hallworth, M. T., & Marra, P. P. (2015). Miniaturized GPS tags identify non-breeding territories of a small breeding migratory songbird. *Scientific Reports*, *5*, 1–6. https://doi.org/10.1038/srep11069

Hersbach, H., Bell, B., Berrisford, P., Biavati, G., Horányi, A., Muñoz Sabater, J., Nicolas, J., Peubey, C., Radu, R., Rozum, I., Schepers, D., Simmons, A., Soci, C., Dee, D., & Thépaut, J. N. (2018a). *ERA5 hourly data on pressure levels from 1979 to present*. Copernicus Climate Change Service (C3S) Climate Data Store (CDS). https://doi.org/10.24381/cds.bd0915c6

Hersbach, H., Bell, B., Berrisford, P., Biavati, G., Horányi, A., Muñoz Sabater, J., Nicolas, J., Peubey, C., Radu, R., Rozum, I., Schepers, D., Simmons, A., Soci, C., Dee, D., & Thépaut, J. N. (2018b). *ERA5 hourly data on single levels from 1979 to present*. Copernicus Climate Change Service Climate Data Store (CDS). https://doi.org/10.24381/cds.adbb2d47

Jonsen, I. D., Basson, M., Bestley, S., Bravington, M. V., Patterson, T. A., Pedersen, M. W., Thomson, R., Thygesen, U. H., & Wotherspoon, S. J. (2013). State-space models for bio-loggers: A methodological road map. *Deep-Sea Research Part II: Topical Studies in Oceanography*, *88–89*, 34–46. https://doi.org/10.1016/j.dsr2.2012.07.008

Jonsen, I. D., Flemming, J. M., & Myers, R. A. (2005). Robust state-space modeling of animal movement data. *Ecology*, *86*(11), 2874–2880. https://doi.org/10.1890/04-1852

Kays, R., Crofoot, M. C., Jetz, W., & Wikelski, M. (2015). Terrestrial animal tracking as an eye on life and planet. *Science*, *348*(6240), aaa2478. https://doi.org/10.1126/science.aaa2478

Kolountzakis, M. N., & Kutulakos, K. N. (1992). Fast computation of the Euclidian distance maps for binary images. *Information Processing Letters*, *43*, 181–184.

Lam, C. H., Nielsen, A., & Sibert, J. R. (2008). Improving light and temperature based geolocation by unscented Kalman filtering. *Fisheries Research*, *91*(1), 15–25. https://doi.org/10.1016/j.fishres.2007.11.002

Leos-Barajas, V., & Michelot, T. (2018). *An introduction to animal movement modeling with hidden Markov models using Stan for Bayesian inference*. http://arxiv.org/abs/1806.10639

Liechti, F., Bauer, S., Dhanjal-Adams, K. L., Emmenegger, T., Zehtindjiev, P., & Hahn, S. (2018). Miniaturized multi-sensor loggers provide new insight into year-round flight behaviour of small trans-Sahara avian migrants. *Movement Ecology*, *6*(1), 1–10. https://doi.org/10.1186/s40462-018-0137-1

Liechti, F., & Bruderer, B. (1995). Direction, speed, and composition of nocturnal bird migration in the south of Israel. *Israel Journal of Zoology*, *41*(3), 501–515. https://doi.org/10.1080/00212210.1995.10688817

Lisovski, S., Bauer, S., Briedis, M., Davidson, S. C., Dhanjal-Adams, K. L., Hallworth, M. T., Karagicheva, J., Meier, C. M., Merkel, B., Ouwehand, J., Pedersen, L., Rakhimberdiev, E., Roberto-Charron, A., Seavy, N. E., Sumner, M. D., Taylor, C. M., Wotherspoon, S. J., & Bridge, E. S. (2020). Light-level geolocator analyses: A user's guide. *Journal of Animal Ecology*, *89*(1), 221–236. https://doi.org/10.1111/1365-2656.13036

Maurer, C. R., Qi, R., & Raghavan, V. (2003). A linear time algorithm for computing exact Euclidean distance transforms of binary images in arbitrary dimensions. *IEEE Transactions on Pattern Analysis and Machine Intelligence*, *25*(2), 265–270. https://doi.org/10.1109/TPAMI.2003.1177156

McClintock, B. T., Langrock, R., Gimenez, O., Cam, E., Borchers, D. L., Glennie, R., & Patterson, T. A. (2020). Uncovering ecological state dynamics with hidden Markov models. *Ecology Letters*, *23*(12), 1878–1903. https://doi.org/10.1111/ele.13610

McKinnon, E. A., Stanley, C. Q., & Stutchbury, B. J. M. (2015). Carry-over effects of nonbreeding habitat on start-to-finish spring migration performance of a songbird. *PLoS ONE*, *10*(11), e0141580. https://doi.org/10.1371/journal.pone.0141580

Meier, C. M., Karaardıç, H., Aymí, R., Peev, S. G., Bächler, E., Weber, R., Witvliet, W., & Liechti, F. (2018). What makes alpine swift ascend at twilight? Novel geolocators reveal year-round flight behaviour. *Behavioral Ecology and Sociobiology*, *72*(3), 45. https://doi.org/10.1007/s00265-017-2438-6

Mills, A. M., Thurber, B. G., MacKenzie, S. A., & Taylor, P. D. (2011). Passerines use nocturnal flights for landscape-scale movements during migration stopover. *Condor*, *113*(3), 597–607. https://doi.org/10.1525/cond.2011.100186

Nielsen, A., Bigelow, K. A., Musyl, M. K., & Sibert, J. R. (2006). Improving light-based geolocation by including sea surface temperature. *Fisheries Oceanography*, *15*(4), 314–325. https://doi.org/10.1111/j.1365-2419.2005.00401.x

Nielsen, A., & Sibert, J. R. (2007). State-space model for light-based tracking of marine animals. *Canadian Journal of Fisheries and Aquatic Sciences*, *64*(8), 1055–1068. https://doi.org/10.1139/F07-064

Nussbaumer, R. (2022). *Flight-Matlab* (1.0.0). https://doi.org/10.5281/zenodo.5883768

Nussbaumer, R., Gravey, M., Briedis, M., & Liechti, F. (2023). Global positioning with animal-borne pressure sensors. *Methods in Ecology and Evolution*. https://doi.org/10.1111/2041-210X.14043

Patterson, T. A., Parton, A., Langrock, R., Blackwell, P. G., Thomas, L., & King, R. (2016). *Statistical modelling of individual animal movement: An overview of key methods and a discussion of practical challenges*. http://arxiv.org/abs/1603.07511

Patterson, T. A., Thomas, L., Wilcox, C., Ovaskainen, O., & Matthiopoulos, J. (2008). State-space models of individual animal movement. *Trends in Ecology & Evolution*, *23*(2), 87–94. https://doi.org/10.1016/j.tree.2007.10.009

Pedersen, M. W., Patterson, T. A., Thygesen, U. H., & Madsen, H. (2011). Estimating animal behavior and residency from movement data. *Oikos*, *120*(9), 1281–1290. https://doi.org/10.1111/j.1600-0706.2011.19044.x

Pennycuick, C. J. (2008). *Modelling the flying bird* (Vol. *5*). Elsevier.

Rabiner, L. R. (1989). A tutorial on hidden Markov models and selected applications in speech recognition. *Proceedings of the IEEE*, *77*(2), 257–286. https://doi.org/10.1109/5.18626

Rakhimberdiev, E., Winkler, D. W., Bridge, E., Seavy, N. E., Sheldon, D., Piersma, T., & Saveliev, A. (2015). A hidden Markov model for reconstructing animal paths from solar geolocation loggers using templates for light intensity. *Movement Ecology*, *3*(1), 25. https://doi.org/10.1186/s40462-015-0062-5

Rhyne, G., & Nussbaumer, R. (2022). *Swainson's warbler multi-sensor light/pressure analysis*. Github Repository. https://github.com/grhyne/SWWA_Pressure

Rime, Y., & Nussbaumer, R. (2022). *Trajectories of northern wheatears breeding in Val Piora*. Github Repository. https://github.com/Rafnuss/Val-Piora-Wheatear

Ross, S. M. (2019). Markov chains. In *Introduction to probability models* (pp. 193–291). Academic Press. https://doi.org/10.1016/B978-0-12-814346-9.00009-3

Royer, F., Fromentin, J., & Gaspar, P. (2005). A state – space model to derive bluefin tuna movement and habitat from archival tags. *Oikos*, *109*(June), 473–484.

Schmaljohann, H., Becker, P. J. J., Karaardic, H., Liechti, F., Naef-Daenzer, B., & Grande, C. (2011). Nocturnal exploratory flights, departure time, and direction in a migratory songbird. *Journal of Ornithology*, *152*(2), 439–452. https://doi.org/10.1007/s10336-010-0604-y

Scott, S. L. (2002). Bayesian methods for hidden Markov models: Recursive computing in the 21st century. *Journal of the American Statistical Association*, *97*(457), 337–351. https://doi.org/10.1198/016214502753479464

Sibert, J. R., Musyl, M. K., & Brill, R. W. (2003). Horizontal movements of bigeye tuna (*Thunnus obesus*) near Hawaii determined by Kalman filter analysis of archival tagging data. *Fisheries Oceanography*, *12*(3), 141–151. https://doi.org/10.1046/j.1365-2419.2003.00228.x

Sjöberg, S., Malmiga, G., Nord, A., Andersson, A., Bäckman, J., Tarka, M., Willemoes, M., Thorup, K., Hansson, B., Alerstam, T., & Hasselquist, D. (2021). Extreme altitudes during diurnal flights in a nocturnal songbird migrant. *Science*, *372*(6542), 646–648. https://doi.org/10.1126/science.abe7291

Sjöberg, S., Pedersen, L., Malmiga, G., Alerstam, T., Hansson, B., Hasselquist, D., Thorup, K., Tøttrup, A. P., Andersson, A., & Bäckman, J. (2018). Barometer logging reveals new dimensions of individual songbird migration. *Journal of Avian Biology*, *49*(9), e01821. https://doi.org/10.1111/jav.01821

Sumner, M. D., Wotherspoon, S. J., & Hindell, M. A. (2009). Bayesian estimation of animal movement from archival and satellite tags. *PLoS ONE*, *4*(10), 19–22. https://doi.org/10.1371/journal.pone.0007324

Taylor, P. D., Crewe, T. L., Mackenzie, S. A., Lepage, D., Aubry, Y., Crysler, Z., Finney, G., Francis, C. M., Guglielmo, C. G., Hamilton, D. J., Holberton, R. L., Loring, P. H., Mitchell, G. W., Norris, D. R., Paquet, J., Ronconi, R. A., Smetzer, J. R., Smith, P. A., Welch, L. J., & Woodworth, B. K. (2017). The motus wildlife tracking system: A collaborative research network to enhance the understanding of wildlife movement. *Avian Conservation and Ecology*, *12*(1). https://doi.org/10.5751/ACE-00953-120108

Thorup, K., Tøttrup, A. P., Willemoes, M., Klaassen, R. H. G., Strandberg, R., Vega, M. L., Dasari, H. P., Araújo, M. B., Wikelski, M., & Rahbek, C. (2017). Resource tracking within and across continents in long-distance bird migrants. *Science Advances*, *3*(1), 1–11. https://doi.org/10.1126/sciadv.1601360

Tobias, J. A., Sheard, C., Pigot, A. L., Devenish, A. J. M., Yang, J., Sayol, F., Neate-Clegg, M. H. C., Alioravainen, N., Weeks, T. L., Barber, R. A., Walkden, P. A., MacGregor, H. E. A., Jones, S. E. I., Vincent, C., Phillips, A. G., Marples, N. M., Montaño-Centellas, F. A., Leandro-Silva, V., Claramunt, S., … Schleuning, M. (2022). AVONET: Morphological, ecological and geographical data for all birds. *Ecology Letters*, *25*(3), 581–597. https://doi.org/10.1111/ele.13898

Viterbi, A. J. (2006). A personal history of the Viterbi algorithm. *IEEE Signal Processing Magazine*, *23*(4), 120–142. https://doi.org/10.1109/MSP.2006.1657823

Werfeli, M., Ranacher, P., & Liechti, F. (2022). Gone with the wind: Inferring bird migration with light-level geolocation, wind and activity measurements. *Methods in Ecology and Evolution*, *2022*(January), 1–10. https://doi.org/10.1111/2041-210x.13837

Wilson, R., Rees, G., & Culik, B. M. (1992). *Estimation of location: Global coverage using light intensity*. https://www.researchgate.net/publication/246098438

Zucchini, W., MacDonald, I. L., & Langrock, R. (2017). *Hidden Markov models for time series*. Chapman and Hall/CRC. https://doi.org/10.1201/b20790

SUPPORTING INFORMATION

Additional supporting information can be found online in the Supporting Information section at the end of this article.

Supporting Information 1. Trajectories (same as Figure 2) and https://doi.org/10.6084/m9.figshare.21731888 for animated GIF.

Supporting Information 2. Wind rose. (same as Figure 3).

Supporting Information 3. Wind support maps. (same as Figure 4).

Supporting Information 4. Histogram of ground, wind, airspeed and flight duration.

Supporting Information 5. Runtime.

How to cite this article: Nussbaumer, R., Gravey, M., Briedis, M., Liechti, F., & Sheldon, D. (2023). Reconstructing bird trajectories from pressure and wind data using a highly optimized hidden Markov model. *Methods in Ecology and Evolution*, *14*, 1118–1129. https://doi.org/10.1111/2041-210X.14082